the plant journal

SEB Society for Experimental Biology

The Plant Journal (2015) **83,** 528–536 doi: 10.1111/tpj.12905

PAY1 improves plant architecture and enhances grain yield in rice

Lei Zhao[1], Lubin Tan[1], Zuofeng Zhu[1], Langtao Xiao[2], Daoxin Xie[3] and Chuanqing Sun[1,*]

[1]*State Key Laboratory of Plant Physiology and Biochemistry, National Center for Evaluation of Agricultural Wild Plants (Rice), Beijing Key Laboratory of Crop Genetic Improvement, Department of Plant Genetics and Breeding, China Agricultural University, Beijing 100193, China,*

[2]*Hunan Provincial Key Laboratory of Phytohormones, Hunan Agricultural University, Changsha, Hunan 410128, China, and*

[3]*MOE Key Laboratory of Bioinformatics, School of Life Sciences, Tsinghua University, Beijing 100084, China*

Received 7 April 2015; revised 28 May 2015; accepted 3 June 2015; published online 10 June 2015.

*For correspondence (e-mail suncq@cau.edu.cn)

SUMMARY

Plant architecture, a complex of the important agronomic traits that determine grain yield, is a primary target of artificial selection of rice domestication and improvement. Some important genes affecting plant architecture and grain yield have been isolated and characterized in recent decades; however, their underlying mechanism remains to be elucidated. Here, we report genetic identification and functional analysis of the *PLANT ARCHITECTURE AND YIELD 1* (*PAY1*) gene in rice, which affects plant architecture and grain yield in rice. Transgenic plants over-expressing *PAY1* had twice the number of grains per panicle and consequently produced nearly 38% more grain yield per plant than control plants. Mechanistically, *PAY1* could improve plant architecture via affecting polar auxin transport activity and altering endogenous indole-3-acetic acid distribution. Furthermore, introgression of *PAY1* into elite rice cultivars, using marker-assisted background selection, dramatically increased grain yield compared with the recipient parents. Overall, these results demonstrated that *PAY1* could be a new beneficial genetic resource for shaping ideal plant architecture and breeding high-yielding rice varieties.

Keywords: *PAY1*, plant architecture, grain yield, polar auxin transport, rice, *Oryza sativa*.

INTRODUCTION

Plant architecture, usually referred to as the three-dimensional organization of the aerial part of a plant, is mainly determined by factors including branching (tillering) pattern, plant height, leaf shape and arrangement, and inflorescence morphology (Reinhardt and Kuhlemeier, 2002; Wang and Li, 2006). Plant architecture is the best means of identifying a plant species, and is also of major agronomic importance as it determines plant survival ability under environmental stress, the suitability of a plant for cultivation, its harvest index and potential grain yield (Peng *et al.*, 1999; Reinhardt and Kuhlemeier, 2002). During the process of crop domestication and improvement, desirable plant architecture was the main selection direction for obtaining high-yielding varieties. For example, the Green Revolution led to dramatic increases in worldwide agricultural productivity since the 1960s from cultivation of lodging-resistant semi-dwarf varieties of wheat and rice (Peng *et al.*, 1999). Therefore, understanding the mechanism underlying plant architecture will facilitate the breeding of crop varieties with high-yield potential.

Rice (*Oryza sativa* L.) is the world's most important cereal crop and feeds half of the world's population. As arable land decreases and global population increases, looking for ways to raise grain yield has become a priority. To meet this challenge, new elite rice varieties with ideal plant architecture that can produce much higher grain yield need to be developed. Rice plant architecture, a comprehensive reflection of important agronomic traits, is mainly determined by tilling pattern, plant height and panicle morphology, and has a decisive effect on grain yield (Wang and Li, 2005, 2008; Xing and Zhang, 2010). In recent years, many important genes/quantitative trait loci controlling plant architecture and grain yield have been isolated and functionally characterized. For example, artificial selection for the *PROSTRATE GROWTH 1* (*PROG1*) mutant during rice domestication led to the transition from the plant

architecture of wild rice to that of domesticated rice, resulting in erect growth, greater grain number and higher grain yield (Jin *et al.*, 2008; Tan *et al.*, 2008). The *DWARF* genes, including *D3*, *D10*, *D14*, *D17*, *D27* and *D53*, have been shown to be involved in the synthesis or signaling pathway of strigolactones, and influence rice tiller number and plant height (Ishikawa *et al.*, 2005; Zou *et al.*, 2005; Arite *et al.*, 2007, 2009; Lin *et al.*, 2009; Jiang *et al.*, 2013; Zhou *et al.*, 2013). *Ghd7* was reported to function in rice growth, development and environmental response, thus regulating rice grain yield, plant height and heading date (Xue *et al.*, 2008; Weng *et al.*, 2014). The *IDEAL PLANT ARCHITECTURE1* (*IPA1*) gene, which encodes *OsSPL14* (SQUAMOSA PROMOTER BINDING PROTEIN-LIKE 14) and is regulated by microRNA (miRNA) OsmiR156, controls rice plant architecture and substantially enhances grain yield (Jiao *et al.*, 2010; Miura *et al.*, 2010). Molecular characterization of genes controlling rice plant architecture and grain yield will not only strengthen our understanding of regulatory mechanisms of these traits, but also aid genetic improvement and breeding of high-yielding rice.

Here, we report the identification of the *PLANT ARCHITECTURE AND YIELD 1* (*PAY1*) gene in rice, which affects plant architecture and grain yield in rice. Our analyses suggest that *PAY1* could affect auxin polar transport and distribution and, as a consequence, optimize plant architecture and increase grain yield in rice. Most interestingly, introduction of *PAY1* can further improve plant architecture and significantly increase grain yield in the background of high-yielding varieties. This study could enhance our understanding of rice plant architecture, and findings concerning *PAY1* will be of value for breeding high-yielding rice.

RESULTS AND DISCUSSION

The *PAY1* mutant displays pleiotropic phenotypes

To identify new regulators of rice plant architecture, a wild rice introgression line YIL55, which displays short plant height, high tillering, thin stems, fewer grains and low yield, was mutagenized with ethyl methane sulfonate to generate a library for genetic screening of mutants with altered plant architecture. We identified a mutant with greatly changed plant architecture, referred to as *PLANT ARCHITECTURE AND YIELD 1* (*PAY1*). Compared with YIL55, the *PAY1* mutant exhibited greater plant height, lower tiller number, smaller tiller angle, thicker stems and larger panicles (Figures 1 and S1). In-depth analysis

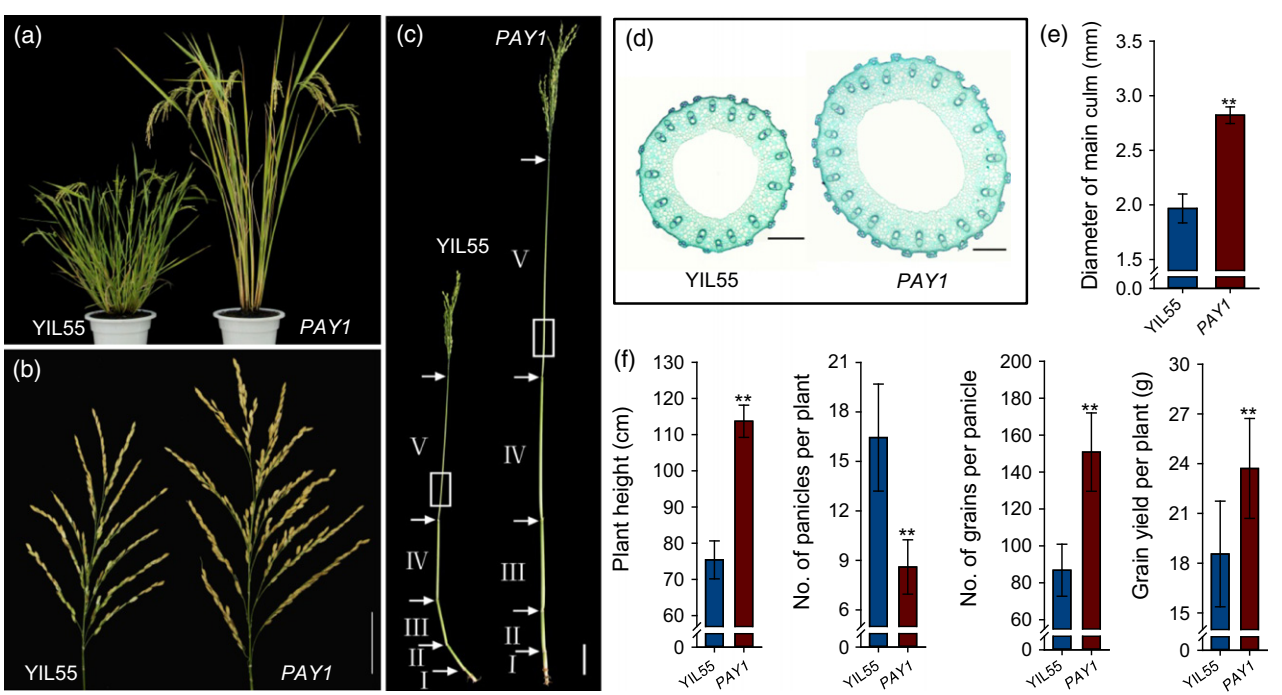

Figure 1. Phenotype of wild-type (YIL55) and *PAY1* mutant.
(a) Introgression line YIL55 and the *PAY1* mutant at maturity stage.
(b) Main panicle of YIL55 and *PAY1* mutant. Scale bar, 5 cm.
(c) Stem structure of YIL55 and *PAY1* mutant. The interval between two arrows showed the length of internode.
(d) Longitudinal sections of the fifth internode (marked by white squares in (c)) between YIL55 and *PAY1* mutant. Scale bars, 200 μm.
(e) The diameter of the fifth internode between YIL55 and *PAY1* mutant. Data are means ± standard deviation (SD) (n = 20).
(f) Comparison of plant height, number of panicles per plant, grain number per panicle and grain yield per plant between YIL55 and *PAY1* mutant plants. Data are means ± SD (n = 30).
In (e) and (f), the double asterisks represent a significant difference determined by Student's t-test at $P < 0.01$.

Figure 2. Molecular identification of *PAY1*.
(a) *PAY1* was mapped in the interval of RM339 and RM223 on the long arm of chromosome 8. *R* is the number of recombinants.
(b) *PAY1* was delimited to a 51-kb region between the sp5 and sp7 markers.
(c) Annotation of the 51-kb region harboring *PAY1* on Nipponbare BAC AP004691.
(d) *PAY1* structure and the mutation site in *PAY1* mutant. The white boxes represent the 5′- and 3′-UTR, the black boxes represent the coding sequences and lines between boxes represent introns. The red asterisk indicates the *PAY1* mutation site.
(e) Gene structure of *PAY1* and constructs used in *PAY1* function investigation. pOE contains *PAY1* ORF (mutation allele) used for overexpression; pRNAi denoted the RNA interference constructs. UBI is a maize *Ubiquitin* promoter.
(f) The phenotype of control plant (CL3) harboring an empty plasmid and *PAY1*-overexpression transgenic plant (pOE6).
(g) Comparison of the main panicle between control plant (CL3) and *PAY1*-overexpression transgenic plants (pOE6). Scale bar, 5 cm.
(h) Relative expression levels of *PAY1* in *PAY1*-overexpression transgenic plants leaves (pOE6 and pOE8) using RT-qPCR analysis.
(i) Comparison of plant height, number of panicles per plant, diameter of main culm, number of grains per panicle and grain yield per plant between control plant (CL3) and *PAY1*-overexpression transgenic plants (pOE6 and pOE8). Data are means ± standard deviation (SD) ($n = 30$).
(j) The phenotype of control plant (CL5) harboring an empty plasmid and RNAi transgenic plant (pRNAi2).
(k) Comparison of the main panicle between control (CL5) and RNAi transgenic plants (pRNAi2). Scale bar, 5 cm.
(l) Relative expression levels of *PAY1* in RNAi transgenic plant leaves (pRNAi2 and pRNAi7).
(m) Comparison of plant height, number of panicles per plant, diameter of main culm, number of grains per panicle and grain yield per plant between control (CL5) and RNAi transgenic plants (pRNAi2 and pRNAi7). Data are means ± SD ($n = 30$). In (i) and (m), the double asterisks represent a significant difference determined by Student's *t*-test at $P < 0.01$.

revealed that the *PAY1* mutant had much longer internodes I–V (Figures 1c and S1a). Microscopy revealed that the elongation of the *PAY1* mutant stem was likely mainly due to an increase in cell size (Figure S1b). Furthermore, *PAY1* mutant showed compact plant architecture with a narrower tiller angle from jointing stage to filling stage, whereas YIL55 had a tiller-spreading phenotype with a wider tiller angle (Figure S1c,d). Further observation showed more vascular bundles in stems of the *PAY1* mutant than of YIL55 (Figure 1e). Interestingly, statistical analysis indicated that the panicles of *PAY1* mutant produced more panicle branches, especially secondary branches (Figure S1e). Most importantly, the *PAY1* mutant had significantly more grains per panicle (73.7%, $P < 0.01$) and grain yield per plant (27.8%, $P < 0.01$) (Figure 1f).

Cloning and characterization of *PAY1*

The F_1 plants from the cross between *PAY1* and YIL55 showed a similar phenotype to the *PAY1* mutant (Figure S2). Of 400 F_2 plants, 304 had a *PAY1*-like phenotype, suggesting a segregation rate of the *PAY1* mutant and YIL55 plants fitting a 3:1 ratio ($\chi^2 = 0.015$; $P = 0.726$). These results indicated that the *PAY1* mutant phenotype was controlled by a single dominant gene.

To clone *PAY1*, we generated an F_2 population of 1100 plants derived from the cross between the *PAY1* mutant and a *japonica* variety Nipponbare, and mapped *PAY1* between the single sequence repeat markers RM339 and RM223 on the long arm of chromosome 8 (Figure 2a). Upon analyses of an additional 4340 F_2 individuals, we further delimited *PAY1* within a 51-kb region between the sp5 and sp7 markers (Figure 2b). Within this region, there were seven predicted genes in the Nipponbare genome (TIGR Rice Genome Annotation Database) (Figure 2c and Table S4). Sequencing the 51-kb mapping region of wild-type YIL55 and mutant *PAY1* revealed a single nucleotide change, G to A, at position +1244 in exon 4 of LOC_Os08g31470. This resulted in a single amino acid substitution from glutamine (Q) in YIL55 to arginine (R) in the *PAY1* mutant (Figures 2d and S3).

To verify whether the altered plant architecture was caused by the single nucleotide change in the LOC_Os08g31470 gene, we generated transgenic YIL55 plants with overexpression of LOC_Os08g31470 cDNA of the *PAY1* mutant (Figure 2e). Real-time quantitative PCR (RT-qPCR) analysis showed that the expression levels of *PAY1* were much higher in transgenic than in control plants (Figure 2h). Consistent with increased *PAY1* expression, all the tested independent over-expressing transgenic lines had similar phenotypes to the *PAY1* mutant–greater plant height, reduced tillers, smaller tiller angle, thicker culms, more panicle branches, more grains per panicle and enhanced grain yield–compared with the control transgenic plants harboring an empty vector (Figures 2f,g,i and S3a).

We further transformed the *PAY1* mutant with the pRNAi construct (Figure 2e). RT-qPCR analysis showed that the expression levels of *PAY1* were down-regulated in RNAi transgenic compared with control plants (Figure 2l). All tested independent RNAi transgenic lines had more tillers, greater tiller angle and marked reductions in plant height, diameter of culms, panicle branches, grains per panicle and grain yield compared with control transgenic plants (Figures 2j,k,m and S3b).

Both the genetic evidence and results of transformation demonstrated that the LOC_Os08g31470 gene corresponded to *PAY1*, and it controlled plant architecture and grain yield in rice.

Sequence analysis of 5′- and 3′-RACE (random amplification of cDNA ends) cDNA products indicated that the *PAY1* cDNA was 2172-bp long, with an open reading frame (ORF) of 1773 bp, a 172-bp 5′-untranslated region (UTR) and a 227-bp 3′-UTR (Figure S4). Further sequence analysis indicated that *PAY1* encoded a protein of 590 amino acids, which contained a peptidase S64 domain, and shared high

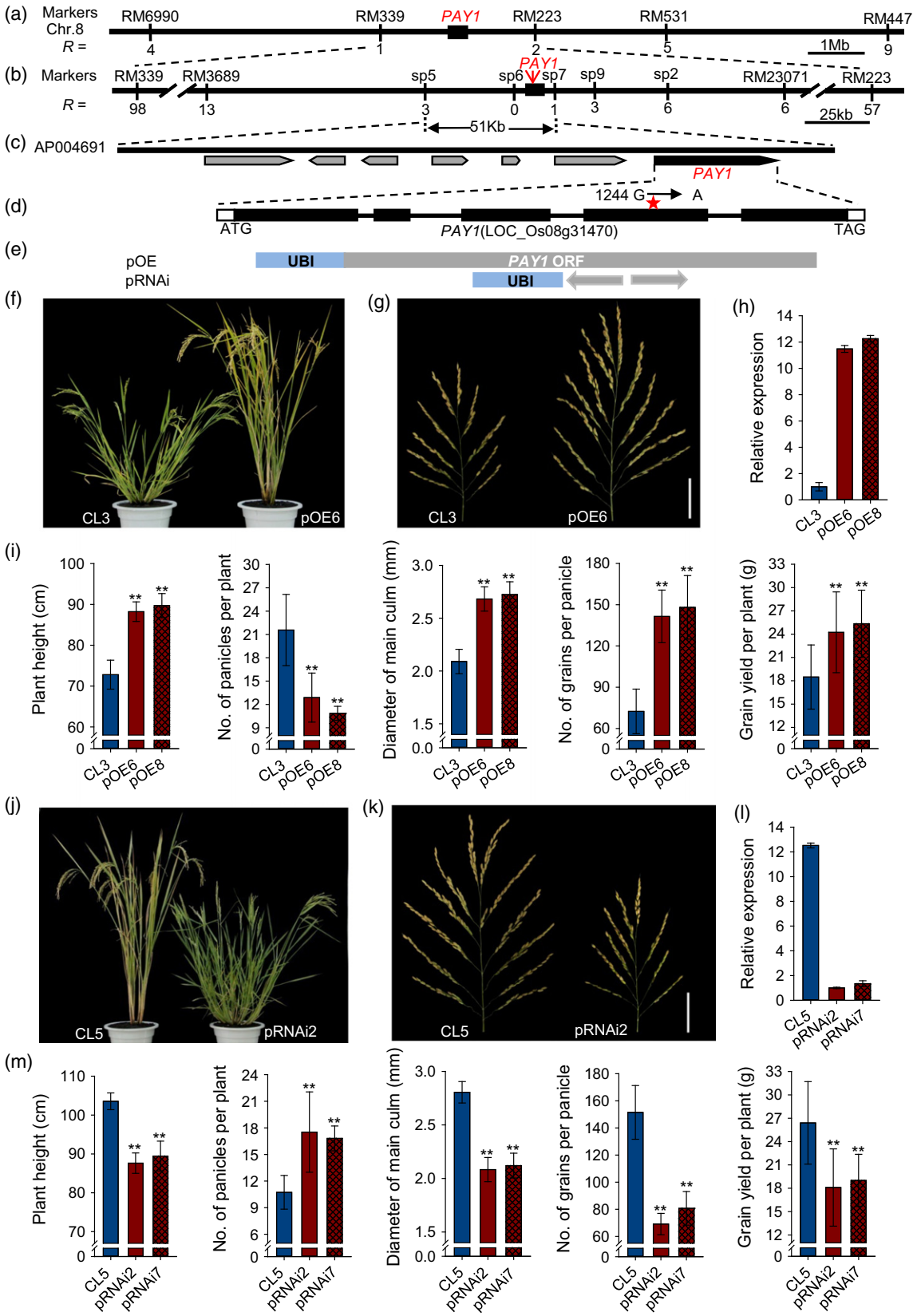

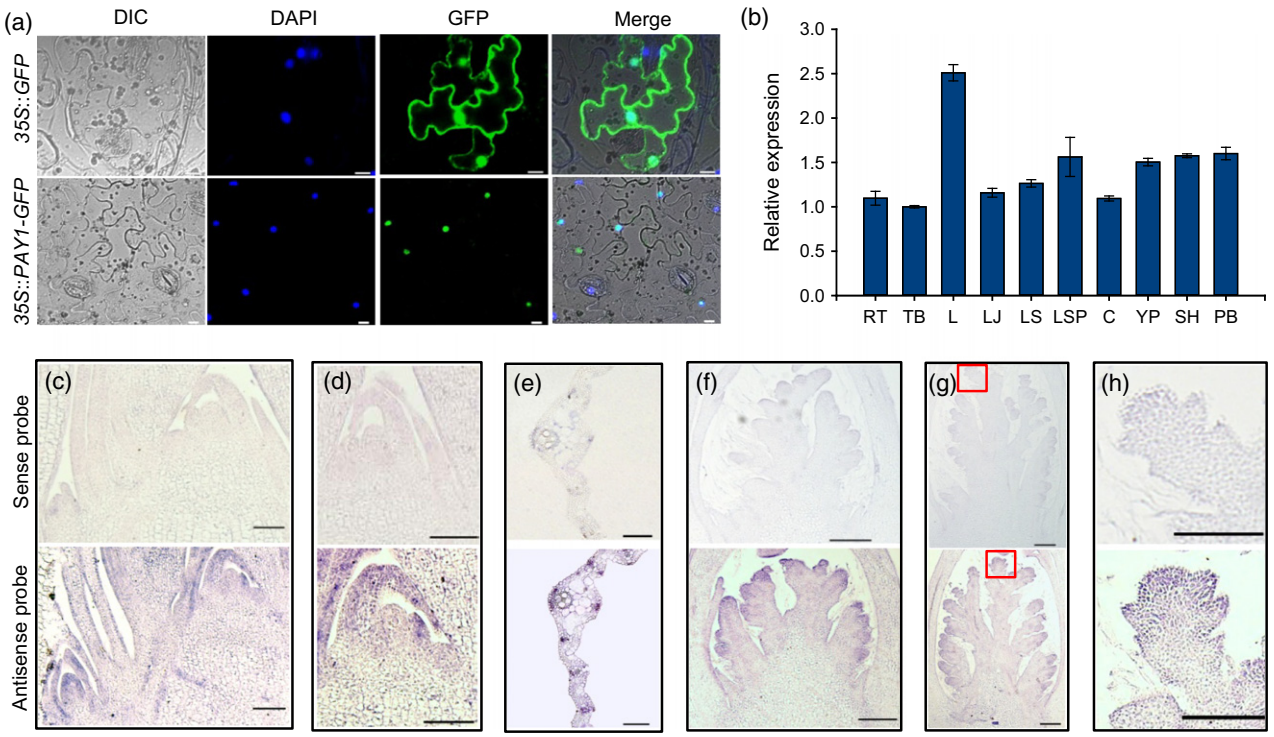

Figure 3. Subcellular localization and expression pattern analysis of *PAY1*.
(a) *PAY1* subcellular localization. *35S::GFP* (top) and *35S::PAY1–GFP* fusion gene (bottom) were transiently expressed in tobacco epidermal cells. The PAY1–GFP fusion protein was exclusively expressed in the nucleus. Scale bars, 100 μm.
(b) The relative expression levels of *PAY1* in various organs. RT, root; TB, tiller base; L, leaf; LJ, lamina joint; LS, leaf sheath; LSP, leaf-sheath pulvinus; C, culm; YP, young panicle; SH, spikelet hull; PB, panicle branch.
(c–h) *PAY1* expression patterns revealed by mRNA *in situ* hybridization. The top panels are sense probes as negative controls, and the bottom panels are antisense probes. (h) was enlarged from (g) marked by red square. Scale bars, 200 μm.

identities with deduced proteins in other plant species including monocots and dicots, such as maize, wheat, barley, tomato and Arabidopsis (Figures S4 and S5). The transient expression experiment in tobacco epidermal cells showed that the PAY1–GFP (green fluorescent protein) fusion protein was specifically localized in the nucleus (Figure 3a).

Expression patterns of *PAY1*

To study the tissue specificity of *PAY1* expression, we introduced a construct consisting of a 1911-bp fragment of the *PAY1* promoter region fused to the GUS reporter gene into the *japonica* cultivar Zhonghua17. GUS staining of transgenic plants indicated that *PAY1* was expressed in almost all organs, including root, leaf, leaf sheath, node, culm, leaf-sheath pulvinus, spikelet hull and panicle branch (Figure S6a–e). Consistent with GUS staining data, RT-qPCR analysis also showed that *PAY1* was ubiquitously expressed in various rice organs, especially leaves (Figure 3b). RNA *in situ* hybridization showed that *PAY1* was predominantly expressed in the leaf primordia, shoot apical meristem, tiller buds, the primordia of primary and secondary branches, and developing spikelets (Figure 3c–h), suggesting that *PAY1* may play critical roles in outgrowth of tiller buds, panicle development and grain production in rice.

The *PAY1* mutant shows reduced polar auxin transport activity

Several decades of studies in different plant species have fully demonstrated that auxin is a determinant of plant architecture, and polar auxin transport (PAT) plays a key role in the regulation of many aspects of plant growth and development (Leyser, 2003; Gallavotti, 2013). To investigate whether *PAY1* was involved in PAT, we compared the basipetal and acropetal indole-3-acetic acid (IAA) transport in etiolated coleoptiles of wild-type and *PAY1* plants. The basipetal IAA transport in *PAY1* was reduced to approximately 41% of that in the wild-type, whereas basipetal transport of ^{3}H-IAA treated with the PAT inhibitor *N*-1-naphthylphtalamic acid (NPA) showed no differences between wild-type and mutant plants (Figure 4a).

To determine whether the reduced basipetal IAA transport activity caused by the mutation in *PAY1* affected the distribution of endogenous IAA, we investigated the endogenous auxin distribution by analyzing GUS expression levels in the transgenic plants for the auxin reporter

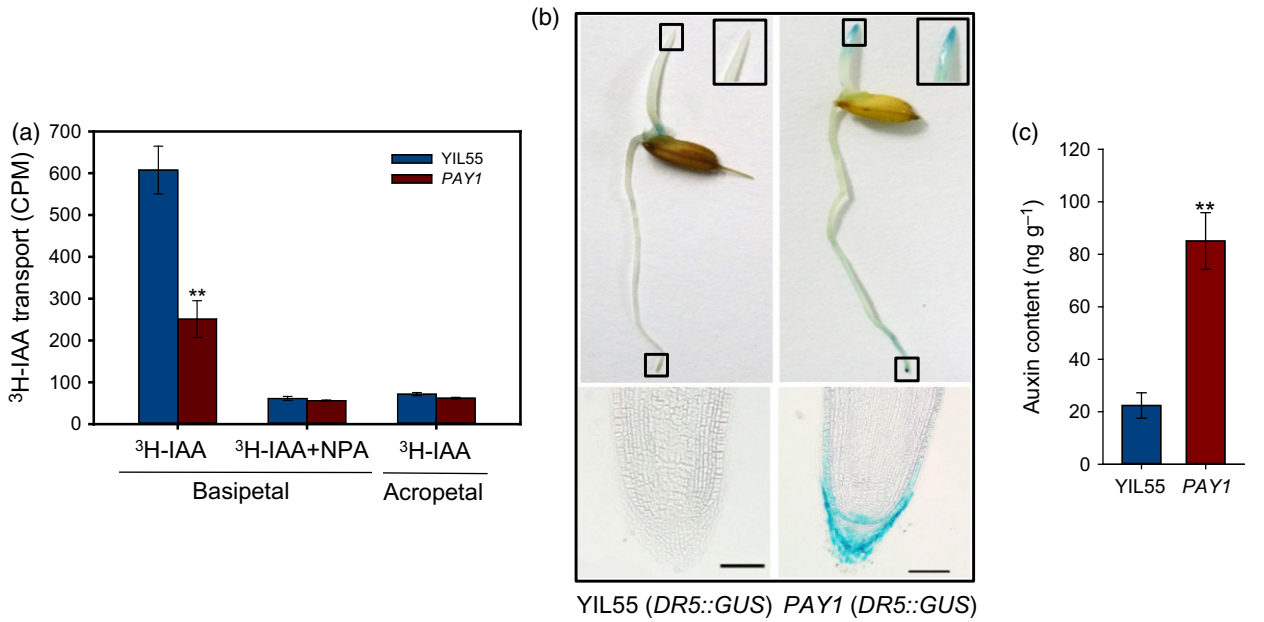

Figure 4. Comparison of auxin biosynthesis and transport between wild-type (YIL55) and *PAY1* plants.
(a) Comparison of PAT between YIL55 and *PAY1* mutant in dark-grown coleoptiles. The acropetal auxin transport measurement was used as a negative control. Values are means ± standard deviation (SD) (n = 5).
(b) *DR5::GUS* expression patterns in dark-grown coleoptiles and roots. Left, *DR5::GUS* within YIL55 background; right, *DR5::GUS* within *PAY1* mutant background. The smaller square in the upper half of panels showed stem apexes of YIL55 and *PAY1* plants, while the larger squares immediately next to it show an enlarged drawing, respectively. The panels below are cross-sections of the root tips shown in panels above, respectively. Scale bars, 100 μm.
(c) Comparison of auxin content in the tip of dark-grown coleoptiles between YIL55 and *PAY1* mutant. Coleoptile fragments 2 mm in length from the tip were used for detection. In (a) and (c), the double asterisks represent a significant difference determined by Student's t-test at $P < 0.01$.

DR5::GUS. Higher GUS expression was detected in the apexes of coleoptiles and root tips in the *PAY1* mutant, but not in YIL55. GUS expression in YIL55 was mainly enriched in the basal part of coleoptiles (Figure 4b). Consistent with the *DR5::GUS* expression pattern, the endogenous auxin (IAA) in the apexes of coleoptiles in *PAY1* mutant was nearly four-fold that in YIL55 (Figure 4c). These results indicated that reduced basipetal IAA transport activity led to altered endogenous IAA distribution in *PAY1* mutant plants, and so affected plant architecture.

PAY1 could potentially be used for high-yield breeding

To evaluate the *PAY1* potential application for optimizing rice plant architecture and increasing grain yields, we introduced the *PAY1* allele into Teqing (TQ) and 9311, two high-yielding *indica* cultivars who harbor the same *pay1* allele to YIL55, to generate the near isogenic lines (NILs) TQ-*PAY1*-NIL and 9311-*PAY1*-NIL, respectively. Compared with recipient plants (TQ and 9311), both TQ-*PAY1*-NIL and 9311-*PAY1*-NIL showed enhanced apical dominance (greater plant height, less tiller number, smaller tiller angle, thicker culms, more secondary branches and larger panicles) and significantly increased grain number per panicle (57.9 and 40.5%, respectively, $P < 0.01$) and grain yield per plant (16.8 and 23.2%, respectively, $P < 0.05$) (Figures 5 and S7). These results indicated that *PAY1* could further enhance the grain yield of currently cultivated rice varieties, and that *PAY1* is a useful allele for shaping ideal plant architecture and increasing grain yield in rice.

In this study, we characterized the *PAY1* gene, which improves plant architecture and enhances grain yield in rice. The dominant *PAY1* gene could significantly optimize plant architecture and increase grain yield in rice, due to altered auxin polar transport and distribution. It is well known that auxin is a central regulator of plant growth and plays a critical role in a wide variety of developmental processes, including embryogenesis, maintenance of apical dominance and formation of lateral organs (Leyser, 2003; McSteen and Leyser, 2005; Vanneste and Friml, 2009). Auxin, produced mainly in the shoot apex, young leaves and root apex, is transported basipetally in the PAT stream, and then inhibits the growth of axillary buds (McSteen and Leyser, 2005; Zhao, 2010; Mashiguchi *et al.*, 2011). Disruption of the auxin gradient, by changing auxin biosynthesis, transport or signaling, will alter organ growth patterns and change plant architecture. Bennett *et al.* (2006) reported that the branching phenotype of *max* mutants in Arabidopsis was caused by increased auxin transport capacity. Arabidopsis *MAP KINAS EKINASE7* (*MKK7*) negatively regulates PAT, thus affecting the formation of plant architecture (Dai *et al.*, 2006). Loss of function of *LAZY1* enhanced PAT and affected lateral auxin transport, thus altering endogenous auxin distribution and resulting in reduced shoot gravitropism and a tiller-spreading

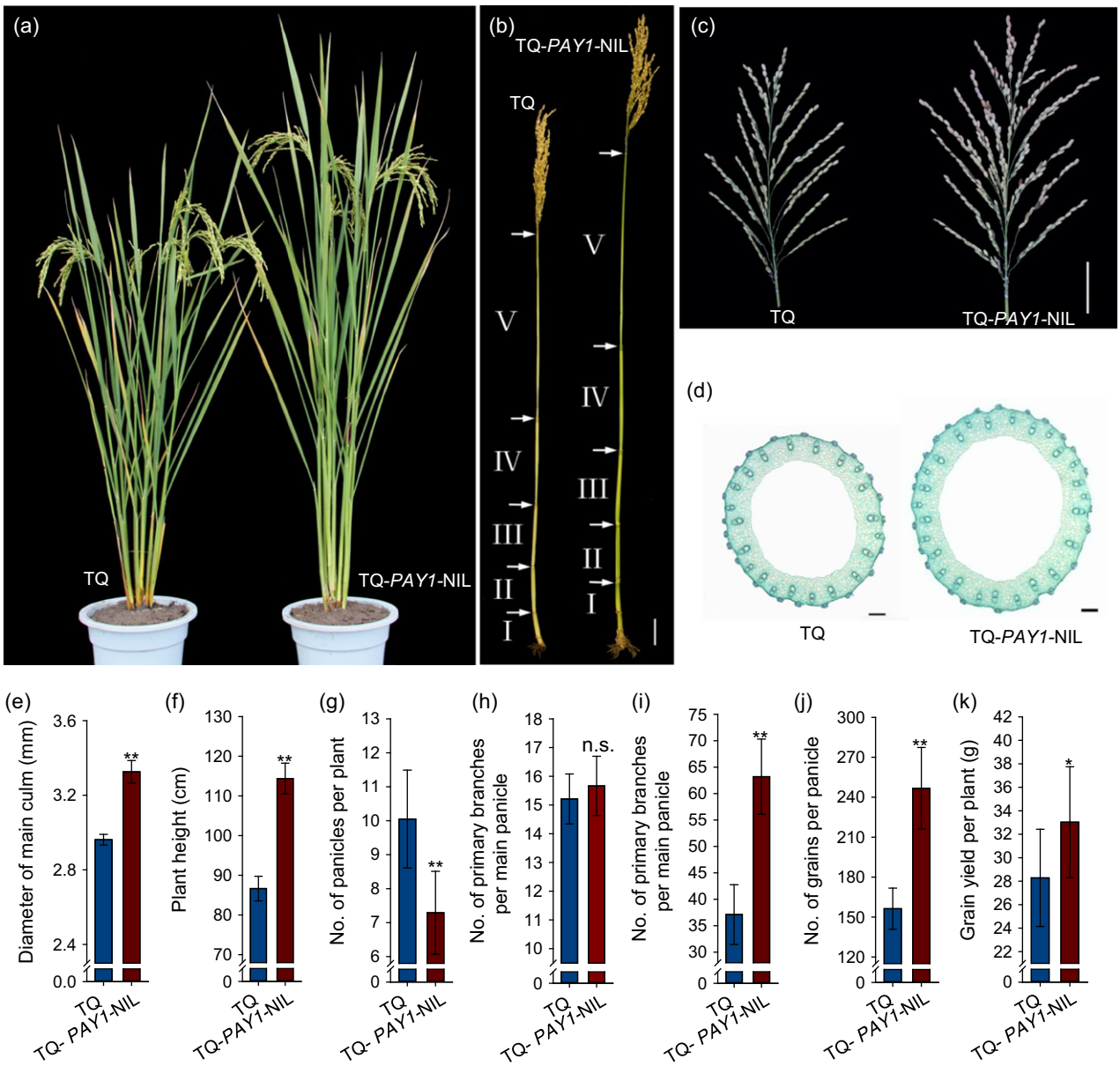

Figure 5. Phenotype of Teqing (TQ) and TQ-*PAY1*-NIL plants.
(a) Gross morphologies of TQ and TQ-*PAY1*-NIL plants at the maturity stage.
(b) Stem structure of TQ (left) and TQ-*PAY1*-NIL (right) plants. The interval between two arrows showed the length of internode.
(c) Comparison of the main panicle between TQ and TQ-*PAY1*-NIL plants. Scale bar, 5 cm.
(d) Cross-sections of the fifth internode between TQ and TQ-*PAY1*-NIL plants. Scale bars, 200 μm.
(e) The diameter of the fifth internode between TQ and TQ-*PAY1*-NIL plants. Data are means ± standard deviation (SD) (n = 20).
(f–k) Comparison of plant height (f), number of panicles per plant (g), number of primary branches per main panicle (h), number of primary branches per main panicle (i), grain number per panicle (j) and grain yield per plant (k) between TQ and TQ-*PAY1*-NIL plants. Data are means ± SD (n = 30). **, Significant at 1% level; *, significant at 5% level; n.s., not significant.

phenotype (Li *et al.*, 2007). The enhanced PAT in *d27* mutant led to increased shoot branching and reduced plant height in rice (Lin *et al.*, 2009). Consistently, the results of the present study revealed that *PAY1* reduced PAT and altered endogenous auxin distribution, leading to a phenotype of enhanced apical dominance with reduced tiller number and angle, and increased plant height in the *PAY1* mutant. The identification of *PAY1* strengthens our understanding of the mechanism by which auxin inhibits the growth of lateral branches and regulates plant architecture in rice.

Improving grain yield has been the primary goal of rice breeding. Rice plant architecture – mainly determined by plant height, tiller number and angle, and panicle morphology – plays a vital role in grain yield formation (Wang and Li, 2008; Xing and Zhang, 2010). Although tremendous

progress has been made in characterizing the genes controlling plant architecture and grain yield in rice, the molecular mechanisms for generating ideal plant architecture and increasing grain yield remain to be elucidated. In the present study, the *PAY1* mutant showed characteristics of ideal plant architecture including reduced tiller number and angle, increased plant height, stem thickness and grain number per panicle compared with the wild-type YIL55. The NILs with Teqing or 9311 genetic background both demonstrated that *PAY1* could shape better plant architecture and enhance grain yield of rice. Overall, our findings show that *PAY1* is an important dominant regulator of rice plant architecture and would be useful for rice genetic improvement and breeding of new varieties with increased grain yield, thus contributing to global food security.

EXPERIMENTAL PROCEDURES

Plant materials

YIL55, the *PAY1* mutant and the segregation population for mapping were grown in paddy fields in Beijing in summer or in Hainan Province in winter. The NILs were generated using continuous backcrossing between *PAY1*, as the donor, and elite *indica* varieties Teqing and 9311, as the recurrent parent. Field-grown selfed progeny of third backcross (BC_3F_3)-generation plants were used for phenotype analysis.

Primers

The primers used in this study are listed in Tables S1–S3.

Genetic confirmation

The entire coding sequence of *PAY1* cDNA (mutation allele), a 1773-bp fragment, was inserted into the vector pCAMBIA1301 driven by the maize *Ubiquitin* promoter to form the overexpression construct pOE. The construct was introduced to *Agrobacterium tumefaciens* strain EHA105 and subsequently transferred into YIL55. There were 18 independent transgenic lines (T_3 generation) harvested, and two lines (pOE6 and pOE8) were used for phenotypic evaluation. The construct pRNAi was generated by the insertion of a hairpin sequence with two 356-bp cDNA inverted repeat fragments targeting the sequence of *PAY1* into pJL1460, driven by the maize *Ubiquitin* promoter. We harvested 13 independent RNAi transgenic lines (T_3 generation) and phenotypically evaluated two of these: pRNAi2 and pRNAi7.

Subcellular localization of PAY1

The construct p*35S::PAY1–GFP* contained *PAY1* fused with *GFP*, driven by a 35S promoter, and introduced into leaf cells of *Nicotiana benthamiana* (a wild Australian tobacco) using *Agrobacterium tumefaciens*-mediated transient transformation by infiltration (Sparkes *et al.*, 2006). Then GFP was visualized in leaf epidermal cells using a Carl Zeiss LSM510 Meta confocal laser scanning microscope (Carl Zeiss AG, http://www.zeiss.com/).

Tissue localization and RNA *in situ* hybridization

The p*PAY1::GUS* construct was transformed into the *japonica* variety Zhonghua17, and the resulting transgenic plants were analyzed by a standard GUS staining assay (Scarpella *et al.*, 2003). RNA *in situ* hybridization assays were performed according to Javelle *et al.* (2011) with some modifications. Shoot apexes and leaves of rice seedlings at the four-leaf stage were fixed with 4% (w/v) paraformaldehyde at 4°C overnight, followed by a series of dehydration and infiltration, and embedded in paraffin (Tissue Path Paraplast Plus, Fisher Scientific). The tissues were sliced into 8-mm sections with a microtome (Leica RM2155; Leica, http://www.leica.com). The 505-bp 3′-region of *PAY1* was subcloned into the pMD18-T vector and used as templates to generate sense and antisense RNA probes. Digoxigenin-labeled RNA probes were prepared using a DIG Northern Starter Kit (Cat. No. 2039672; Roche, http://www.roche.com), according to the manufacturer's instructions.

RT-qPCR and RACE analysis

For RT-qPCR analysis, total RNA was extracted from various samples using TRIzol reagent (Invitrogen, http://www.lifetechnologies.com) and was purified using the RNeasy Micro Kit (Qiagen, http://www.qiagen.com). First-strand cDNA was synthesized to using oligo(dT)18 primer (TaKaRa) and SuperScript® III Reverse Transcriptase (Invitrogen) from 3 μg of total RNA. The expression levels of *PAY1* and other genes were analyzed using a CFX96 Real-Time System (Bio-Rad, http://www.bio-rad.com) and rice *Ubiquitin* gene as an internal control. Each set of experiments was repeated three times, and the relative quantification method ($2^{-\Delta\Delta C_T}$) used to evaluate quantitative variation. 5′- and 3′-RACE was carried out using a 5′-Full RACE Kit with tobacco acid pyrophosphatase (TAP) and 3′-Full RACE Core Set with PrimeScript™ reverse transcriptase (RT) (TaKaRa, http://www.takara.com) following the manufacturer's instructions.

PAT assay

PAT assays were performed according to Li *et al.* (2007) with some minor modifications. Five groups of six 5-day-old dark-grown coleoptile segments (0.2 cm away from the tip) of 2 cm length were used for the assay. The segments were incubated in 1/2 Murashige and Skoog (MS; pH 5.8) liquid medium with shaking at 100 rpm for 2 h to remove endogenous IAA. The apical or basal ends of the coleoptile segments (for basipetal or acropetal transport assays, respectively) were then placed in a 200-μl microcentrifuge tube with one end submerged in 10 μl of ½MS liquid medium containing 0.35% phytogel, 500 nM [^{3}H] IAA and 500 nM free IAA in darkness at room temperature for 2 h. NPA was applied to the media as indicated. The unsubmerged ends of the segments (0.5 cm in length) were excised and washed three times with ½MS liquid medium. After 20 h incubation in 2 ml of scintillation liquid, the radioactivity of each section was counted by a liquid scintillation counter (1450 MicroBeta TriLux; Perkin-Elmer, http://www.perkinelmer.com).

Measurement of free IAA content

IAA extraction and measurement were performed using liquid chromatography-mass spectrometry (LC-MS) according to Kowalczyk and Sandberg (2001) with some modifications. The tips (0.2 cm in length) of 3-day-old dark-grown coleoptiles were harvested and used for the assay. After extraction and purification, the samples were subjected to LC-MS analysis using a liquid scintillation counter (1450 MicroBeta TriLux, http://www.perkinelmer.com).

ACCESSION NUMBERS

Data deposition: The *PAY1* sequence reported in this paper was deposited in the GenBank database accession no. KP233774 (full-length cDNA).

ACKNOWLEDGEMENTS

This research was supported by the National Natural Science Foundation of China (No. 91335202, No. 30930057), the China National High-tech Research and Development ('863') Program (No. 2012AA10A301).

SUPPORTING INFORMATION

Additional Supporting Information may be found in the online version of this article.

Figure S1. Phenotype of wild-type (YIL55) and *PAY1* mutant.

Figure S2. Phenotypic characterization of F_1 plants derived from the cross between YIL55 and *PAY1* mutant.

Figure S3. Full-length cDNA of *pay1* from wild-type (YIL55) and the deduced amino acid sequence.

Figure S4. Phenotype of control plant and transgenic plant.

Figure S5. Phylogeny of the PAY1 protein family.

Figure S6. Expression pattern of *PAY1.*

Figure S7. Phenotype of 9311 and 9311-*PAY1*-NIL plants.

Table S1. Primers used for mapping of *PAY1.*

Table S2. Primer sequences used to generate constructs.

Table S3. Primers used for RACE, RT-qPCR and RNA *in situ* hybridization.

Table S4. Information on predicted genes in the fine mapping region of *PAY1.*

REFERENCES

Arite, T., Iwata, H., Ohshima, K., Maekawa, M., Nakajima, M., Kojima, M., Sakakibara, H. and Kyozuka, J. (2007) *DWARF10,* an *RMS1/MAX4/DAD1* ortholog, controls lateral bud outgrowth in rice. *Plant J.* **51**, 1019–1029.

Arite, T., Umehara, M., Ishikawa, S., Hanada, A., Maekawa, M., Yamaguchi, S. and Kyozuka, J. (2009) *d14,* a strigolactone-insensitive mutant of rice, shows an accelerated outgrowth of tillers. *Plant Cell Physiol.* **50**, 1416–1424.

Bennett, T., Sieberer, T., Willett, B., Booker, J., Luschnig, C. and Leyser, O. (2006) The *Arabidopsis MAX* pathway controls shoot branching by regulating auxin transport. *Curr. Biol.* **16**, 553–563.

Dai, Y., Wang, H., Li, B., Huang, J., Liu, X., Zhou, Y., Mou, Z. and Li, J. (2006) Increased expression of MAP KINASE KINASE7 causes deficiency in polar auxin transport and leads to plant architectural abnormality in *Arabidopsis. Plant Cell*, **18**, 308–320.

Gallavotti, A. (2013) The role of auxin in shaping shoot architecture. *J. Exp. Bot.* **64**, 2593–2608.

Ishikawa, S., Maekawa, M., Arite, T., Onishi, K., Takamure, I. and Kyozuka, J. (2005) Suppression of tiller bud activity in tillering dwarf mutants of rice. *Plant Cell Physiol.* **46**, 79–86.

Javelle, M., Marco, C.F. and Timmermans, M. (2011) *In situ* hybridization for the precise localization of transcripts in plants. *J. Vis. Exp.* **57**, e3328.

Jiang, L., Liu, X., Xiong, G. *et al.* (2013) DWARF53 acts as a repressor of strigolactone signalling in rice. *Nature*, **504**, 401–405.

Jiao, Y., Wang, Y., Xue, D. *et al.* (2010) Regulation of *OsSPL14* by OsmiR156 defines ideal plant architecture in rice. *Nat. Genet.* **42**, 541–544.

Jin, J., Huang, W., Gao, J.P., Yang, J., Shi, M., Zhu, M.Z., Luo, D. and Lin, H.X. (2008) Genetic control of rice plant architecture under domestication. *Nat. Genet.* **40**, 1365–1369.

Kowalczyk, M. and Sandberg, G. (2001) Quantitative analysis of indole-3-acetic acid metabolites in *Arabidopsis. Plant Physiol.* **127**, 1845–1853.

Leyser, O. (2003) Regulation of shoot branching by auxin. *Trends Plant Sci.* **8**, 541–545.

Li, P., Wang, Y., Qian, Q., Fu, Z., Wang, M., Zeng, D., Li, B., Wang, X. and Li, J. (2007) *LAZY1* controls rice shoot gravitropism through regulating polar auxin transport. *Cell Res.* **17**, 402–410.

Lin, H., Wang, R., Qian, Q. *et al.* (2009) DWARF27, an iron-containing protein required for the biosynthesis of strigolactones, regulates rice tiller bud outgrowth. *Plant Cell*, **21**, 1512–1525.

Mashiguchi, K., Tanaka, K., Sakai, T. *et al.* (2011) The main auxin biosynthesis pathway in *Arabidopsis. Proc. Natl Acad. Sci. USA*, **108**, 18512–18517.

McSteen, P. and Leyser, O. (2005) Shoot branching. *Annu. Rev. Plant Biol.* **56**, 353–374.

Miura, K., Ikeda, M., Matsubara, A., Song, X.J., Ito, M., Asano, K., Matsuoka, M., Kitano, H. and Ashikari, M. (2010) O*sSPL14* promotes panicle branching and higher grain productivity in rice. *Nat. Genet.* **42**, 545–549.

Peng, J., Richards, D.E., Hartley, N.M. *et al.* (1999) 'Green Revolution' genes encode mutant gibberellin response modulators. *Nature*, **400**, 256–261.

Reinhardt, D. and Kuhlemeier, C. (2002) Plant architecture. *EMBO Rep.* **3**, 846–851.

Scarpella, E., Rueb, S. and Meijer, A. (2003) The *RADICLELESS1* gene is a required for vascular pattern formation in rice. *Development*, **130**, 645–658.

Sparkes, I., Runions, J., Kearns, A. and Hawes, C. (2006) Rapid, transient expression of fluorescent fusion proteins in tobacco plants and generation of stably transformed plants. *Nat. Protoc.* **1**, 2019–2025.

Tan, L., Li, X., Liu, F. *et al.* (2008) Control of a key transition from prostrate to erect growth in rice domestication. *Nat. Genet.* **40**, 1360–1364.

Vanneste, S. and Friml, J. (2009) Auxin: a trigger for change in plant development. *Cell*, **136**, 1005–1016.

Wang, Y. and Li, J. (2005) The plant architecture of rice (*Oryza sativa*). *Plant Mol. Biol.* **59**, 75–84.

Wang, Y. and Li, J. (2006) Genes controlling plant architecture. *Curr. Opin. Biotechnol.* **17**, 123–129.

Wang, Y. and Li, J. (2008) Molecular basis of plant architecture. *Annu. Rev. Plant Biol.* **59**, 253–279.

Weng, X., Wang, L., Wang, J., Hu, Y., Du, H., Xu, C., Xing, Y., Li, X., Xiao, J. and Zhang, Q. (2014) *Grain number, plant height, and heading date7* is a central regulator of growth, development, and stress response. *Plant Physiol.* **164**, 735–747.

Xing, Y. and Zhang, Q. (2010) Genetic and molecular bases of rice yield. *Annu. Rev. Plant Biol.* **61**, 421–442.

Xue, W., Xing, Y., Weng, X. *et al.* (2008) Natural variation in *Ghd7* is an important regulator of heading date and yield potential in rice. *Nat. Genet.* **40**, 761–767.

Zhao, Y. (2010) Auxin biosynthesis and its role in plant development. *Annu. Rev. Plant Biol.* **61**, 49–64.

Zhou, F., Lin, Q., Zhu, L. *et al.* (2013) D14-SCFD3-dependent degradation of D53 regulates strigolactone signaling. *Nature*, **504**, 406–410.

Zou, J., Chen, Z., Zhang, S., Zhang, W., Jiang, G., Zhao, X., Zhai, W., Pan, X. and Zhu, L. (2005) Characterizations and fine mapping of a mutant gene for high tillering and dwarf in rice (Oryza sativa L.). *Planta*, **222**, 604–612.